Lecture 7. More on BL wind profiles

Stability

Above the surface layer, the wind profile is also affected by stability. As we mentioned previously, unstable BLs tend to have much more well-mixed wind profiles than stable BLs. The figures below show observations from the Wangara experiment on how the velocity defect laws and temperature profile are altered by BLstability (as measured by h/L). Within stability classes, the velocity profiles collapse when scaled with a velocity scale u_* and the observed BL depth h, but there is a large difference between the stability classes.

Baroclinicity

We would expect baroclinicity (vertical shear of geostrophic wind) to also affect the observed wind profile. This is most easily seen for an Ekman layer in a geostrophic wind with constant vertical shear:

$$\mathbf{u}_g(z) = (G + Mz, Nz), \quad \text{where} \quad M = -(g/fT_0)\partial T/\partial y, \; N = (g/fT_0)\,\partial T/\partial x$$

$$-f(v - Nz) = \nu\, d^2u/dz^2$$

$$f(u - G - Mz) = \nu\, d^2v/dz^2$$

$$u(0) = 0, \; u \rightarrow G + Mz \; \text{ as } z \rightarrow \infty$$

$$v(0) = 0, \; v \rightarrow Nz \; \text{ as } z \rightarrow \infty$$

Resultant BL velocity profile just has thermal wind added onto it:

$$u(z) = G(1 - e^{-\zeta}\cos\zeta) + Mz$$

$$v(z) = G\,e^{-\zeta}\sin\zeta + Nz \quad (\zeta = z/\delta, \; \delta = (2\nu/f)^{1/2})$$

This can considerably alter the BL wind profile. The largest crossing angle of the surface wind direction across the isobars is seen if $M < 0$, $N > 0$,corresponding to surface cold advection. This effect is clearly seen in the figure below of crossing angle vs. thermal wind orientation in 23000 wind profiles over land (Hoxit 1974). On weather maps, one can see much larger crossing angles behind cold fronts than ahead of them. On the other hand, the wind turns less with height if $N > 0$ (surface cold advection)

Turbulence Profiles (Garratt 3.3)

For applications such as the dispersion of pollutants, it is important to understand the characteristics of turbulence in different types of BL. LES simulations illustrate some of these characteristics. Most of the figures below are from Moeng and Sullivan (1994, *JAS*, **51**, 999-1022).

Neutral BLs

Moeng and Sullivan simulated a neutral BL capped by a strong (8 K) inversion at a height of $z_i = 500$ m. The geostrophic wind is 15 m s^{-1} in the $+x$ direction and $u_* = 0.5$ m s^{-1}. The figures on 4.1.4 show x-y slices of u' at various heights, and the wind hodograph. Because of the capping inversion, the wind shear within the bulk of the BL is fairly small (nearly a mixed layer), with strong wind shear across the inversion.

Garratt

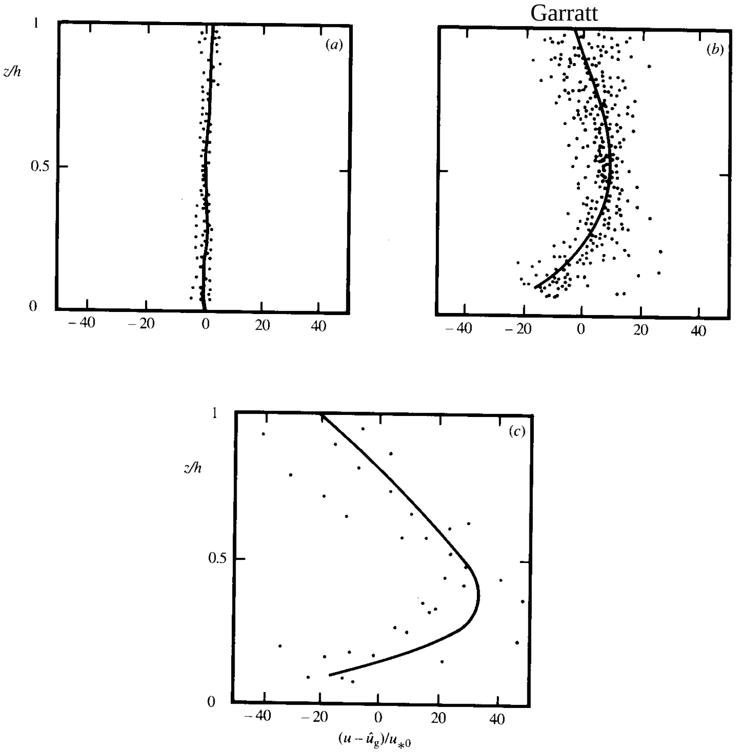

Fig. 3.13 Profiles of the normalized velocity defect for the u-component as a function of normalized height z/h, based on Eq. 3.82 and an analysis of Wangara observations. Three stability regimes are presented: (a) $-150 < h/L < -120$; (b) $0 < h < 30$; (c) $180 < h/L < 210$. Curves are drawn by eye. After Yamada (1976), *Journal of Atmospheric Sciences*, American Meteorological Society.

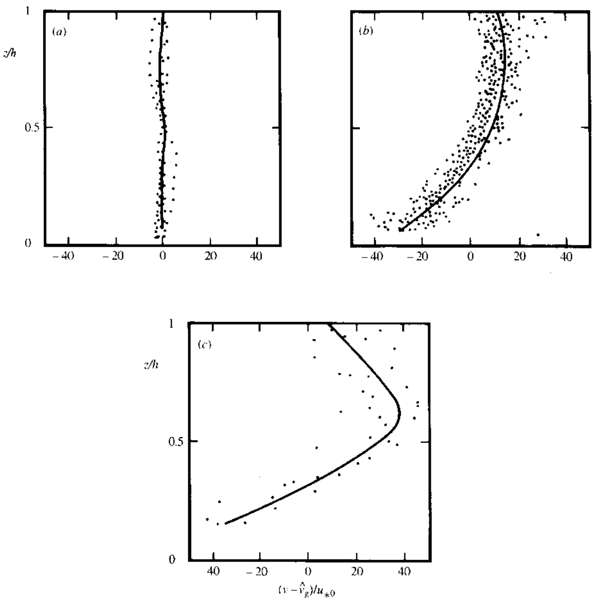

Same for v

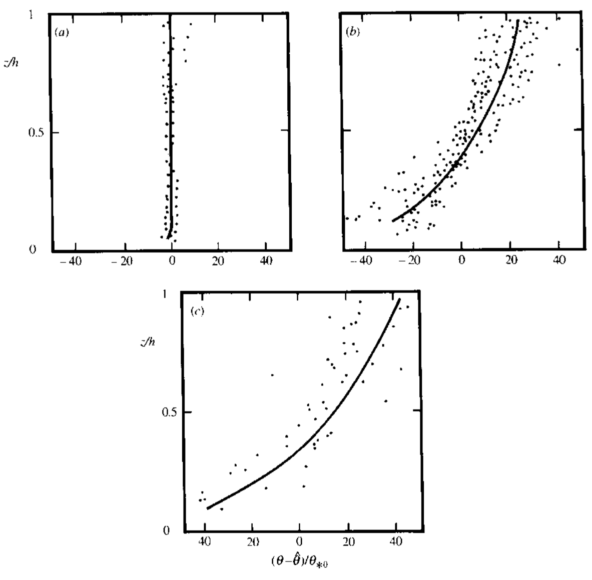

Same for θ

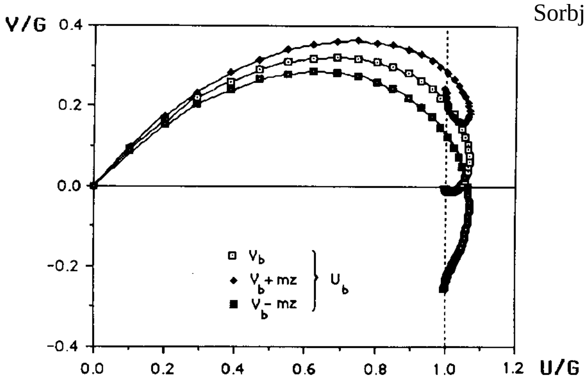

Sorbjan

Figure 6.11 Ekman spirals obtained for the baroclinic correction of the V component of the wind velocity, $a = 0.001$, $m = 0.0001$. Points are plotted every 100 m, starting on the surface. U_b, V_b-barotropic components of the wind vector. Dotted line shows directions of the thermal wind vectors.

Ekman spirals for thermal wind with $M = 0$ and $N > 0$, $N = 0$ (no thermal wind), $N < 0$. Near-surface wind is oriented more in $+y$ direction (larger crossing angle) for $N > 0$.

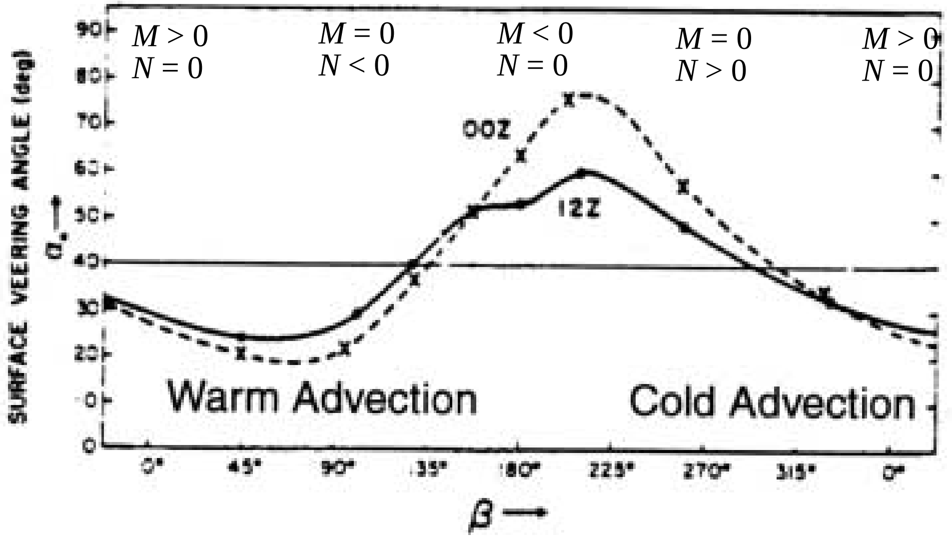

Isobaric crossing angle of surface wind vs. angle of thermal wind. Afternoon (00 Z) soundings show stronger effect due to stronger vertical mixing in a more convective BL (Hoxit 1974)

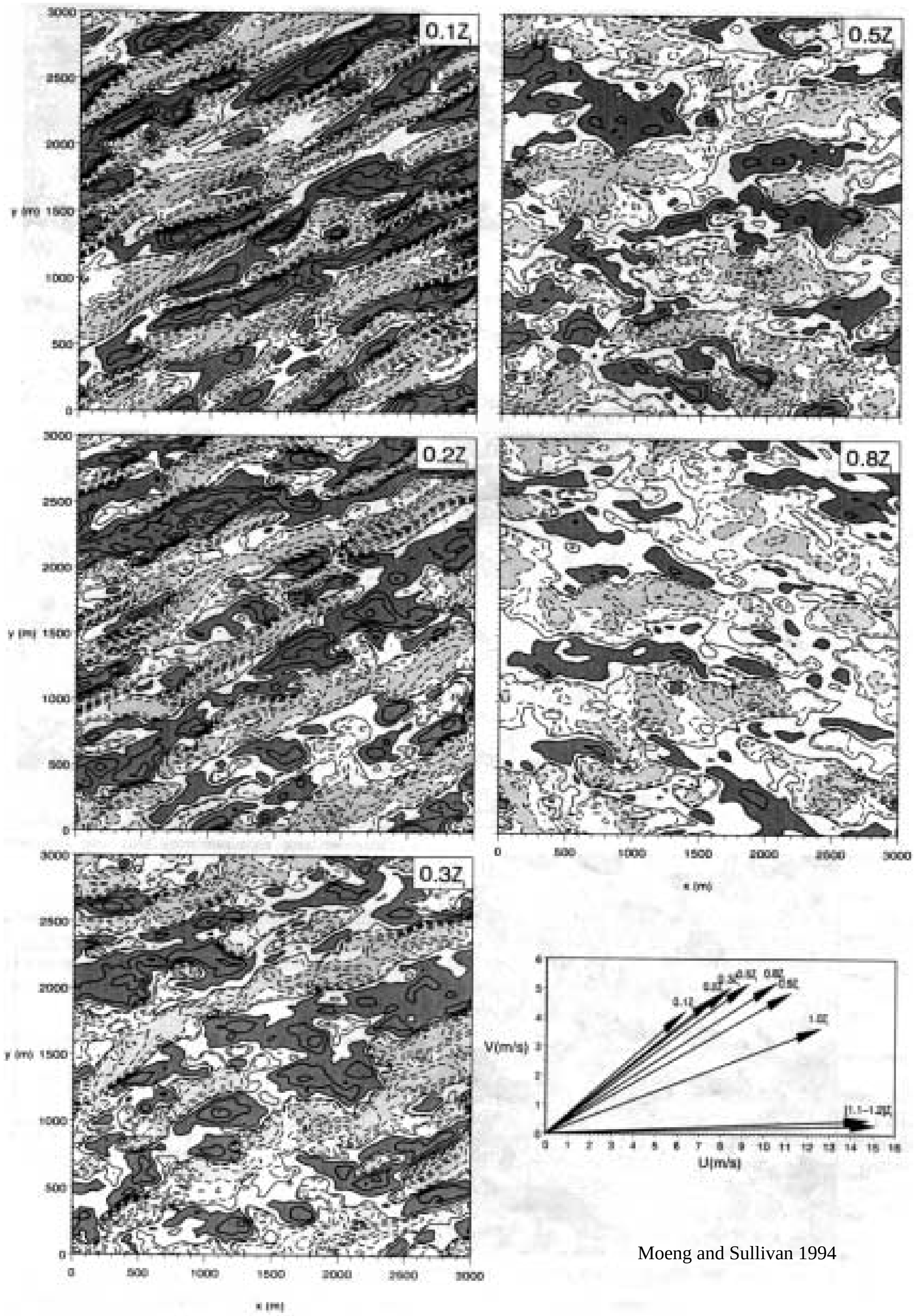

Moeng and Sullivan 1994

FIG. 3. Contours of *u* in the *x*–*y* plane at five height levels for simulation S and its wind hodograph: contours (−3, −2.5, −2, −1.5, −1, −0.5, −0.1, 0.1, 0.5, 1, 1.5, 2, 2.5), dark (light) shading values larger (smaller) than 0.5 (−0.5).

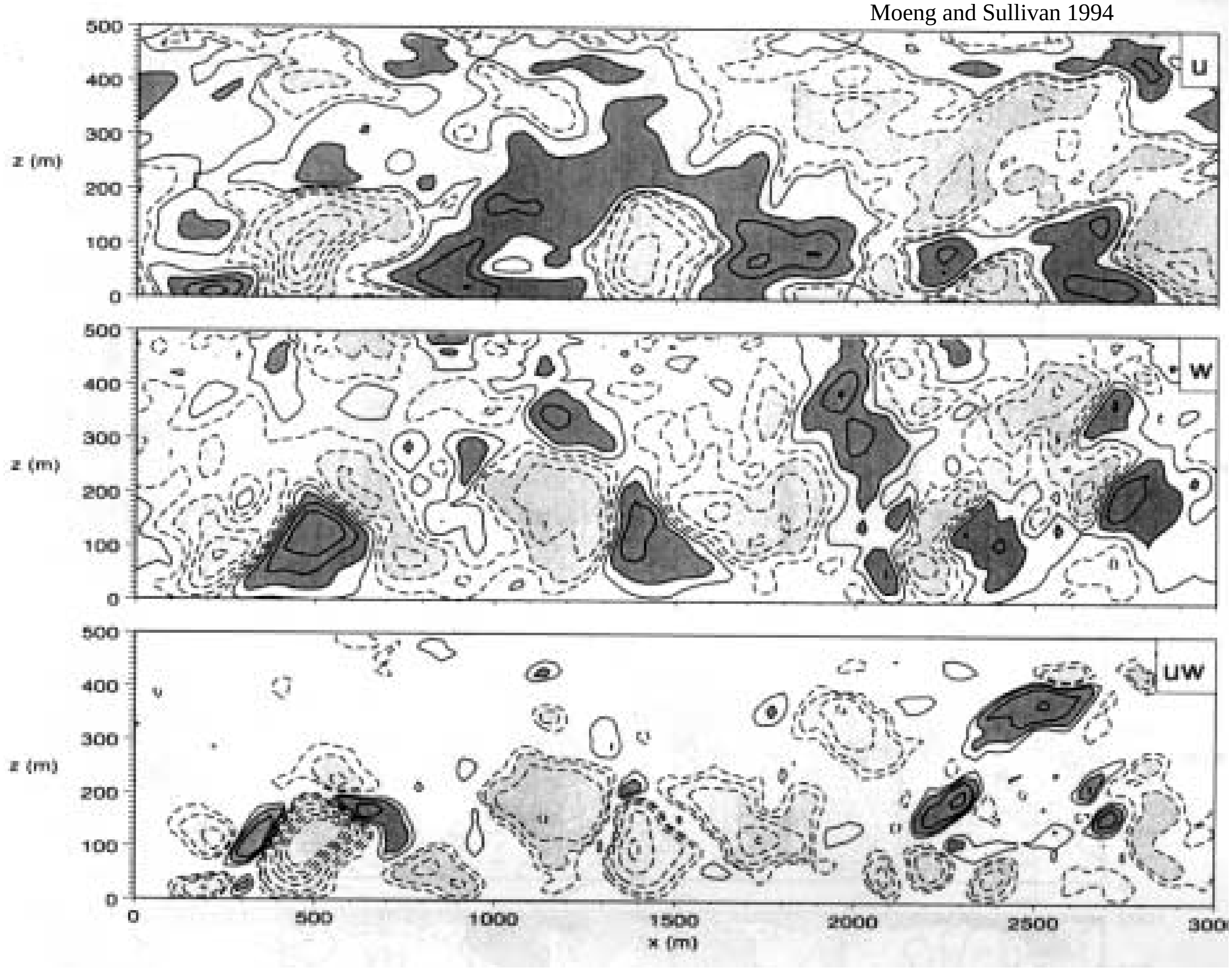

Moeng and Sullivan 1994

Vertical section through a neutral BL.Note strong anticorrelation between u' and w'.

We can see that at the top of the surface layer ($z/z_i = 0.1$) , u' is organized in streaks, corresponding to long cylindrical eddies or ‘rolls’ oriented about 20° to the left of the geostrophic wind. The wind perturbations weaken and become less linearly organized with height. The figure below shows an *x-z* cross section of u', w', and $u'w'$ across the center of the domain in *y*. Here one can see the strong negative correlation between u' and w' (updrafts have a small *u* than downdrafts), especially for $z/z_i < 0.5$. In fact, the correlation coefficient between u', w' is -0.4 at below this level.

The variances of the three velocity components are shown on the next page, along with their counterparts for a convective BL. For a neutral BL, they are all strongest near the ground, with the strongest perturbations in *u* at all levels. Their sum, divided by two, is the TKE profile. As we have discussed already, the TKE budget is essentially a balance between shear production (most of which occurs in the lowest 20% of the BL where shear and momentum fluxes are both largest) and turbulent dissipation, with little contribution from turbulent transport.

Although there is no surface buoyancy flux, the turbulence does erode the capping inversion, creating a small downward entrainment buoyancy flux $\overline{w'b'}_i$. In fact, we find that

$$\overline{w'b'}_i = -u_*^3/z_i$$

If we assume that the whole boundary layer is warmed equally by entrainment of warm air from

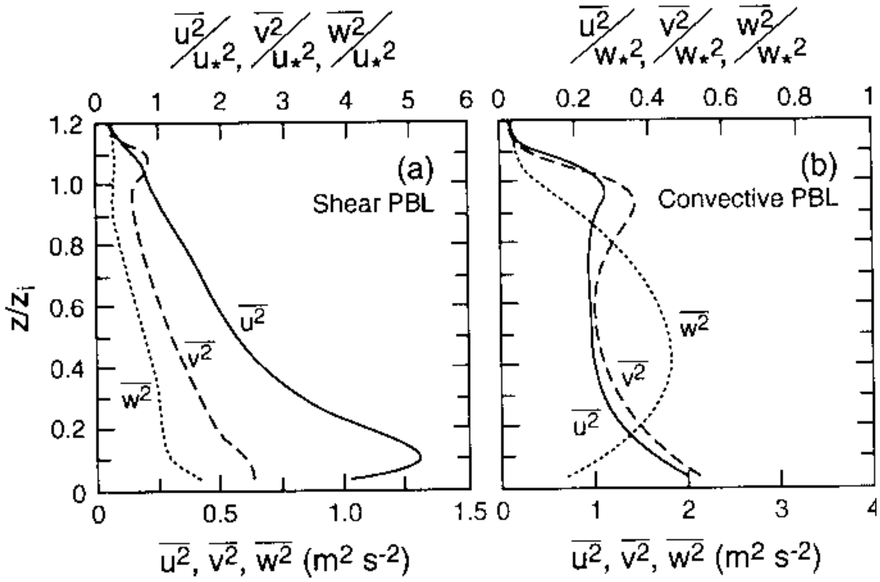

Moeng and Sullivan 1994

FIG. 9. Vertical distributions of the velocity variances of simulations S and B.

above the inversion, we can associate a buoyancy flux profile with the entrainment which varies linearly from 0 at $z = 0$ to $\overline{w'b'}_i$ at the inversion. The consumption rate of TKE by this buoyancy flux, vertically averaged over the BL, is $\overline{w'b'}_i/2 = -0.5u_*^3/z_i$. If we compare this to the overall dissipation rate of TKE, we find that the TKE dissipation rate is much larger than this at the surface but about $2u_*^3/z_i$ in the upper part of the BL; i. e. entrainment is consuming around 25% of the TKE generated in this region.

Weakly Unstable BLs

Moeng and Sullivan also simulated a weakly unstable boundary layer , also under a capping inversion. This was similar to their neutral case, but with a surface hear flux of 50 W m $^{-2}$, giving an Obuhkov length $L = -300$ m comparable to z_i. In this case (page 4.1.7), the streaky structure is still apparent at the lowest levels, but large convective rolls dominate the turbulence higher in the BL and help keep it well-mixed. The buoyant and shear contributions to TKE are comparable in this case. A velocity scale based on surface buoyancy flux can be derived from the TKE equation.

$$w_* = (B_0 z_i)^{1/3}$$

(Note that $z_i/L = -kw_*^3/u_*^3$); for this case $w_* = 0.9$ m s^{-1}. For the buoyancy and shear driven BL a combined velocity scale $w_m^3 = 5u_*^3 + w_*^3$ seems to work best. In particular, with any combination of surface buoyancy flux and shear, Moeng and Sullivan found that the entrainment buoyancy flux is roughly

$$\overline{w'b'}_i = -0.2\, w_m^3/z_i$$

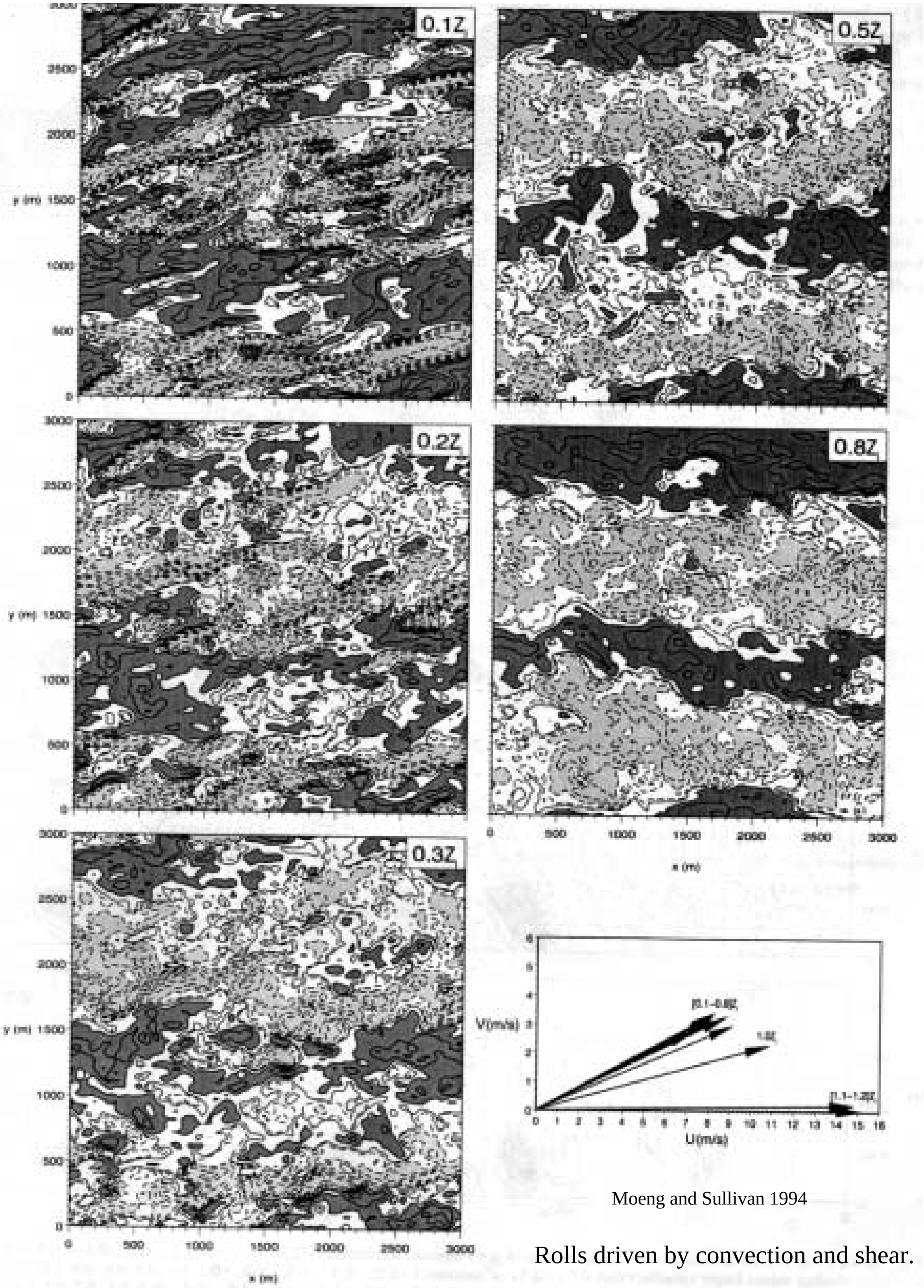

Moeng and Sullivan 1994

Rolls driven by convection and shear.

FIG. 15. Views of x–y for simulation SB1 for u field at five height levels and its wind hodograph: contours (−3, −2.5, −2, −1.5, −1, −0.5, −0.1, 0.1, 0.5, 1, 1.5, 2), dark (light) shading values larger (smaller) than 0.5 (−0.5). Some height labels in the wind hodograph are grouped since winds at those levels are about the same.

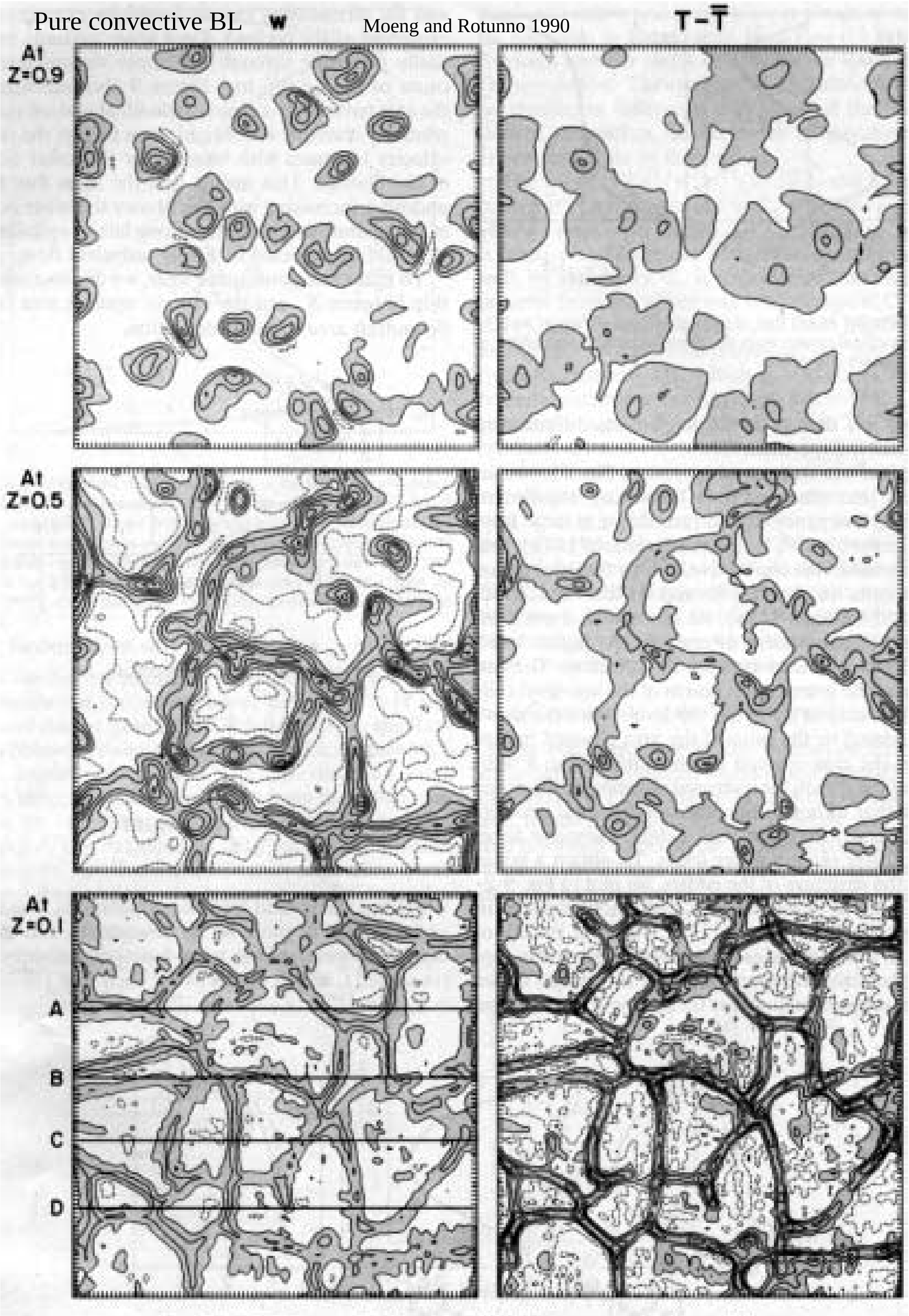

FIG. 8. As in Fig. 3, except for Experiment H. Vertical cross sections through the locations marked A, B, C and D are shown in Fig. 9.

Convective BLs

Lastly, let’s look at a purely buoyancy-driven or convective BL. The simulations shown (Moeng and Rotunno 1990, *JAS*) are below a rigid boundary and do not include entrainment, but do show the overall structure well. At the bottom, there is a very good correlation between w' and θ', with polygonal regions of updraft separating circular patches of downdraft. As we move close to the BL top, the updrafts accelerate and combine to become circular, and the temperature fluctuations become much less well correlated with the updrafts. For penetrative convection, in fact the updrafts would be a bit cooler than the surrounding air at the highest level shown.

The velocity variances (previous page) show a very different structure than for a shear-driven BL. They are dominated by the large eddies, which have updrafts in the middle of the BL and predominantly lateral motions at its top and bottom. There is much more velocity variance in the upper part of the BL, so the TKE and TKE dissipation rate are almost uniform with height and equal to $0.4w_*^3/z_i$. As in the upper part of a shear-driven BL , about 25% of the TKE generated is going into consumption by entrainment, which averaged over the BL is $\overline{w'b'}_i/2 = 0.1w_*^3/z_i$. .

Below are shown LES simulations (Sullivan et al. 1998, *JAS*) of the top of a convective BL penetrating a moderate inversion of 4 K (grid resolution at top right of each plot). White indicates $\theta < 304$ K, other shades increasing θ up to 308 K. Arrows indicate velocity in the x-z plane. Plots show a sequence of times 10 s apart. Note the undulations in the BL top, with downward moving air on the edge of hummocks where updraft air has partly mixed with free-tropospheric air. These motions produce the negative buoyancy flux in the entrainment zone, which for a pure convective BL reaches $-0.2B_0$. Also note in panels e-h the formation of an ‘entrainment tongue’ at x = 1750 m of partly mixed, buoyant air that is getting sucked into the BL.